

Surface plasmon-mediated photoluminescence boost in graphene-covered CsPbBr₃ quantum dots

Youngsin Park^{a, 1}, Elham Oleiki^{a,1}, Guanhua Ying^b, Atanu Jana^c, Mutibah Alanazi^b, Vitaly Osokin^b, Sangeun Cho^c, Robert A. Taylor^{b,*}, Geunsik Lee^{a,*}

^a Department of Chemistry, College of Natural Science, Ulsan National Institute of Science and Technology, Ulsan 44919, Korea

^b Clarendon Laboratory, Department of Physics, University of Oxford, Parks Road, Oxford OX1 3PU, UK

^c System Semiconductor Science, Dongguk University, Seoul 04620, Korea

ABSTRACT:

The optical properties of graphene (Gr)-covered CsPbBr₃ quantum dots (QDs) were investigated using micro-photoluminescence spectroscopy, revealing a remarkable three-orders-of-magnitude enhancement in photoluminescence (PL) intensity compared to bare CsPbBr₃ QDs. To elucidate the underlying mechanisms, we combined experimental techniques with density functional theory (DFT) calculations. DFT simulations showed that the graphene layer generates interfacial electrostatic potential barriers when in contact with the CsPbBr₃ surface, impeding carrier leakage from

* Corresponding author:

E-mail address: robert.taylor@physics.ox.ac.uk (R. Taylor), gslee@unist.ac.kr (G. Lee)

¹ These authors contributed equally to this work.

perovskite to graphene and enhancing radiative recombination. Additionally, graphene passivates CsPbBr₃ surface defect states, suppressing nonradiative recombination of photo-generated carriers. Our study also revealed that graphene becomes n-doped upon contact with CsPbBr₃ QDs, activating its plasmon mode. This mode resonantly couples with photo-generated excitons in the perovskite. The momentum mismatch between graphene plasmons and free-space photons is resolved through plasmon scattering at Gr/CsPbBr₃ interface corrugations, facilitating the observed super-bright emission. These findings highlight the critical role of graphene as a top contact in dramatically enhancing CsPbBr₃ QDs' PL. Our work advances the understanding of graphene-perovskite interfaces and opens new avenues for designing high-efficiency optoelectronic devices. The multifaceted enhancement mechanisms uncovered provide valuable insights for future research in nanophotonics and materials science, potentially leading to breakthroughs in light-emitting technologies.

Keywords: Perovskite quantum dots, Graphene coating, Photoluminescence, Surface plasmon-induced resonance, Defect passivation.

1. Introduction

All inorganic lead halide perovskites (LHP) CsPbX_3 ($X = \text{Cl, Br or I}$) have emerged as promising materials for a wide range of optoelectronic applications such as solar cells [1,2], light-emitting diodes [3], and photodetectors [4] due to their higher stability compared to their organic-inorganic counterparts [5-7]. Among these, CsPbBr_3 has excellent optoelectronic properties, including an extremely high photoluminescence (PL) quantum yield, narrow emission bandwidth, and long carrier diffusion length and lifetime [8,9]. Furthermore, the emission energy can be tuned from 2.29 eV to 2.53 eV by synthesizing it in various structures such as bulk single crystals, thin films, nanocrystals (NCs), nanowires, and QDs [10-12], offering versatility in device design and application. CsPbBr_3 nanostructure emission could originate from various sources, including a single exciton, lasing due to biexcitonic emission [13], cavity lasing from a micro/nanowire [14], triplet excitonic emission [15], and superfluorescence [16]. Enhancing the optoelectronic properties of LHPs through heterojunction formation has been a focus of recent research. In particular, graphene (Gr), with its ultrahigh carrier mobility [17] and wavelength-independent light absorption [18], has been hybridized with CsPbBr_3 to improve its performance [4,19,20]. Previous studies have reported enhanced visible light absorption in CsPbBr_3 -NCs/Gr heterostructures [19,20] and improved photoresponse due to facilitated electron transfer from CsPbBr_3 to graphene [4,19]. However, these configurations often led to PL quenching, limiting their potential in light-emitting applications. Surface defects in LHPs can introduce nonradiative trap states, significantly affecting their PL properties [21-23]. Various approaches have been

explored to passivate these defects, including the application of different functional molecules [24]. Notably, encapsulating MAPbBr₃ NCs with Gr was shown to passivate surface defect states, enhancing PL intensity by a factor of seven [25]. Another effective method to improve the quantum efficiency of optoelectronic heterojunctions is PL enhancement through the resonant excitation of surface plasmons [26-28]. For Gr/semiconductor interfaces, it has been reported that a Gr plasmon can be resonantly activated by radiative recombination of electron-hole pairs from a semiconductor photo absorber, leading to enhanced PL through interaction with interface corrugations [29-32]. In this study, we present a novel approach to dramatically enhance the PL intensity of CsPbBr₃ QDs by covering them with Gr, achieving a three orders of magnitude increase. We employ a comprehensive set of experimental techniques, including μ -PL measurements and transmission electron microscopy (TEM), complemented by density functional theory (DFT) calculations to elucidate the underlying mechanisms. Crucially, we demonstrate that the configuration of Gr-covered CsPbBr₃ QDs (Gr/CsPbBr₃/SiO₂) leads to the formation of interfacial electrostatic potential barriers, which inhibit carrier leakage from the perovskite to the graphene layer. This is in stark contrast to the previously reported CsPbBr₃/Gr/SiO₂ configuration, where PL quenching was observed due to electron transfer from CsPbBr₃ to Gr [19].

2. Experimental section

2.1 Materials and Methods

In a 100 ml glass bottle, Cs₂CO₃ (0.0325 g, 0.01 mmol) was placed into a 15 mL glass vial with 2 mL 1-octadecene (ODE) and 1 mL oleic acid (OA), then dried at 120 °C for

1 hour until all Cs_2CO_3 had reacted with OA and kept it for 3 hr. In another glass vial, PbBr_2 (0.073 gm, 0.02 mmol) and n-octylammonium bromide (OAmBr) (0.042 gm, 0.2 mmol) were dissolved in 1 mL DMF and 2 mL of ODE at 120 °C and kept for 3 hr. Subsequently, 3 mL Cs-oleate solution was injected into the lead precursor solution, resulting in a change of solution color to greenish yellow. The crude solution was centrifuged for 5 minutes at 5000 rpm after cooling to room temperature. The residue was redispersed in toluene by sonication and again centrifuged at 5000 rpm for 5 min. The obtained product was washed with 2 ml of methyl acetate and subjected to another centrifugation at 10000 rpm for 10 minutes. Finally, the product was dried in a vacuum oven at 60 °C for 12 hours. The CsPbBr_3 QDs were put in a toluene solution and the solution was treated under sonication for 10 min. Then the solution was dispersed on a SiO_2 (300 nm)/Si substrate. Then the graphene was transferred on the CsPbBr_3 dispersed SiO_2 substrate. The PMMA-coated Gr prepared on a Cu foil was placed in a solution of Cu etchant (CE-100, Transene Company, Inc.) to remove the Cu foil. After the Cu foil was completely removed away, the PMMA-coated Gr was scooped using the CsPbBr_3 dispersed SiO_2 . The PMMA layer was then removed with acetone, and the sample was rinsed several times with deionized water.

2.2 Structural Characterization.

Transmission electron microscopy images were taken on a JEOL JEM-2100F electron microscope using a 200kV electron source. Samples were prepared on 200-mesh carbon coated Cu grids by dropping NC solutions which were allowed to evaporate.

2.3 Laser system and optical photoluminescence.

A 100 fs frequency-doubled Ti:sapphire laser operating at 400 nm with a repetition rate of 80 Mhz was used as the excitation source. The incident laser power on the CsPbBr₃ surface ranged from a few nW to a few tens of μW. The sample was mounted in a continuous-flow helium cryostat, allowing the temperature to be controlled accurately from 4.2 K to room temperature. Measurements were performed at cryogenic temperatures to resolve any fine structure, since its energy is small compared to the thermal bath at room temperature. The CsPbBr₃ nanocrystals in a toluene solution were dispersed on an Au patterned SiO₂ substrate to determine the position of nanocrystals with different sizes. The optical properties were characterized using a fiber-based confocal micro-photoluminescence (μPL) setup. A 100× long working distance apochromatic objective was held by a sub-micron precision piezoelectric stage above the cryostat and used to focus the incident laser beam to a spot size of ~1 μm² and to collect the resulting luminescence. The luminescence was then directed to a 0.3 m focal length spectrometer with a 600 gr/mm grating. The signal was finally detected using a cooled charge coupled device (CCD) detector. A telecentric lens arrangement was also present allowing the incident angle of the exciting laser at the entrance to the objective to be varied by a computer-controlled mirror thus providing an independent means to move the exiting spot relative to the collected emission, which is imaged confocally through the center of the objective. Time resolved photoluminescence (TRPL) measurements were carried out using the same experimental set up as above. The dispersed PL was reflected towards a photomultiplier connected to a commercial

photon counting system. Measurements of the lifetimes of the confined states were then carried out over a range of excitation power densities.

2.4 Density functional theory calculations

DFT calculations were performed using the Vienna *ab initio* simulation package based on the plane wave pseudopotential approach [33], and by using a Generalized gradient approximation (GGA) within PBE parameterization [34] as the exchange-correlation functional. To incorporate van der Waals interactions, dispersion correction was added to the total energy and forces by employing the Tkatchenko and Scheffler (TS) approach [35]. To model the CsPbBr₃ layer, we first optimized the atomic structure of the bulk CsPbBr₃ cubic phase using the experimental lattice parameter of 5.87 Å [36]. Then we used the optimized bulk unit cell and designed four different (001) CsPbBr₃ slabs considering both CsBr and PbBr₂ surface terminations [35,37]. To have distinguishable contributions from surface and bulk states in the electronic structure, we repeated the unit cell 7 times along the [001] direction and optimized all atomic positions. Also, to gain the lowest amount of lattice mismatch in heterostructure supercells, we employed $2 \times \sqrt{2} \times \sqrt{2}$ unit cells of 2D-CsPbBr₃, 7×2 rectangular layer of Gr, and 4×2 unit cells of SiO₂ composed of 4 atomic layers along [001] direction. We made the SiO₂ slab from its cubic bulk structure with the lattice parameter of 4.93 Å. The lattice mismatch values for CsPbBr₃, Gr, and SiO₂ are 0.8%, 6%, and 30%, respectively. To avoid spurious interactions between the periodic images of heterostructures we inserted 15 Å of vacuum along [001] direction and optimized all the atomic positions except two bottom layers of SiO₂ by using a single Γ -point. The kinetic energy cutoff was set

to 400 eV while convergence criteria of 10^{-4} eV and 0.05 eV/Å were employed for energies and forces, respectively.

3. Results and Discussion

The detailed crystal structure of the individual CsPbBr₃ QDs was investigated using TEM. Figure 1a shows TEM images of the CsPbBr₃ QDs, revealing that the QDs tend to aggregate, forming clusters of various sizes. In contrast to previous reports of well-aligned CsPbBr₃ QDs [8,38-44], our QDs exhibit a random distribution ranging from approximately 10 to 50 nm, as shown in high-resolution TEM images (Fig. 1b). Despite this random size distribution, 60–70% of the QDs within each cluster are aligned in the same direction. When we measured the PL, we dispersed the QD clusters with a size of ~ 2 μm on the SiO₂ substrates. The schematic diagram of the micro PL system is depicted (Fig. 1c). The PL from these QD clusters may exhibit complex optical properties. While individual QDs in the cluster might emit independently, leading to a reduction in overall coherence, the close proximity of QDs within each cluster could potentially lead to collective effects. These effects might include exciton coupling or energy transfer between neighboring QDs, which could influence the emission characteristics. Furthermore, the orientation of QDs within a cluster, if sufficiently aligned, might contribute to some degree of directional emission. However, given the random distribution of QD sizes and orientations observed in the TEM images, the exact nature of these optical properties requires further investigation through detailed spectroscopic measurements and theoretical modeling. The resulting PL emission may exhibit complex characteristics, potentially including some degree of coherence and

directionality, depending on the specific arrangement and interactions within each cluster. Like other semiconductor QDs, the size and geometry for a matrix of CsPbBr₃ QDs are subject to some extent of variations. Although the spin coating process has helped to spatially filter the QD clusters based on their sizes, we often found that clusters of similar dimensions are clumped together. It is therefore possible to excite multiple QD arrays under slightly different conditions within a single laser spot. In most cases, the QD clusters produce independent signals given their distinct emission centers. However, clusters with very similar geometric formations or even two closely alike matrices of QDs within a single cluster may be in close proximity, causing their individual collective behaviors to overlap and interact with each other.

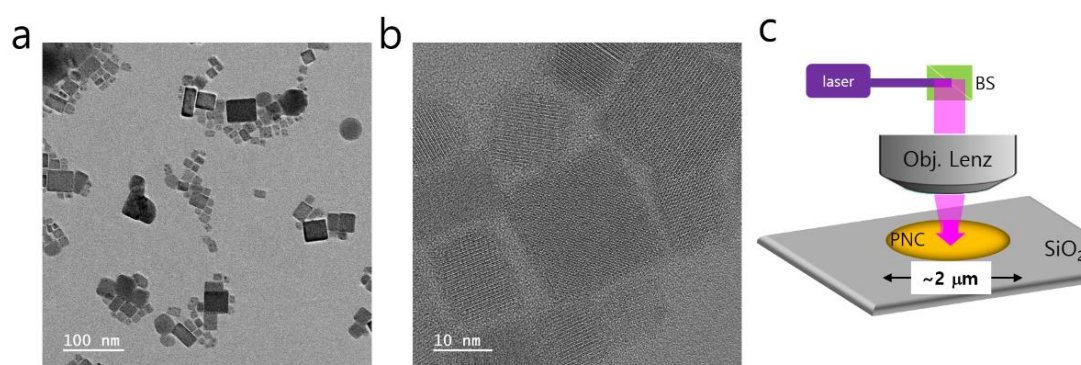


Fig. 1. (a) TEM image of CsPbBr₃ QD clusters, showing aggregation of individual QDs into various sized clusters. Scale bar: 100 nm. (b) High-resolution TEM image of individual QDs within a cluster, revealing the crystal structure and size distribution ranging from ~10 to 50 nm. Scale bar: 10 nm. (c) Schematic diagram of the μPL setup. The laser beam is focused on a CsPbBr₃ QD cluster with a diameter of ~2 μm on a SiO₂ substrate. BS represents the beam splitter, and Obj. indicates the objective used to focus the laser and collect the emitted light.

Figure 2 presents excitation power-dependent PL spectra for bare and Gr-covered CsPbBr₃ QDs, measured at low temperature. For bare CsPbBr₃ QDs (Fig. 2a), a single excitonic emission peak at 2.33 eV with a full width at half maximum (FWHM) of ~8 meV is observed at the lowest excitation fluence of 31.8 μJ/cm². As excitation fluence increases, new blue-shifted emission lines emerge, and the integrated intensity shows an S-shaped behavior (Fig. S1a), indicating stimulated emission. In contrast, Gr-covered CsPbBr₃ QDs (Fig. 2b) exhibit multiple emission peaks even at a low excitation fluence of 6 nJ/cm², with significantly enhanced PL intensity and signal-to-noise ratio. No new peaks emerge or blue-shift below excitation fluences of a few tens of μJ/cm². The integrated PL intensity increases linearly with excitation fluence (Fig. S1b). On the other hand, the PL intensity of the CsPbBr₃/Gr/SiO₂ heterostructure is quenched (Fig. 2c), consistent with the previous reports [4,19,20]. Even at excitation power of 0.16 kJ/cm², the spectrum is very noisy and broad with an FWHM of ~5 meV and the intensity doesn't increase much at high excitation power of 2.7 kJ/cm². Figure 2d compares PL spectra for the three different heterostructures, demonstrating significant PL enhancement in the Gr-covered structure despite the absence of stimulated emission peaks. To investigate the origin of the PL intensity quenching, we explored the electronic structure of the CsPbBr₃/Gr heterostructure by performing the DFT calculations.

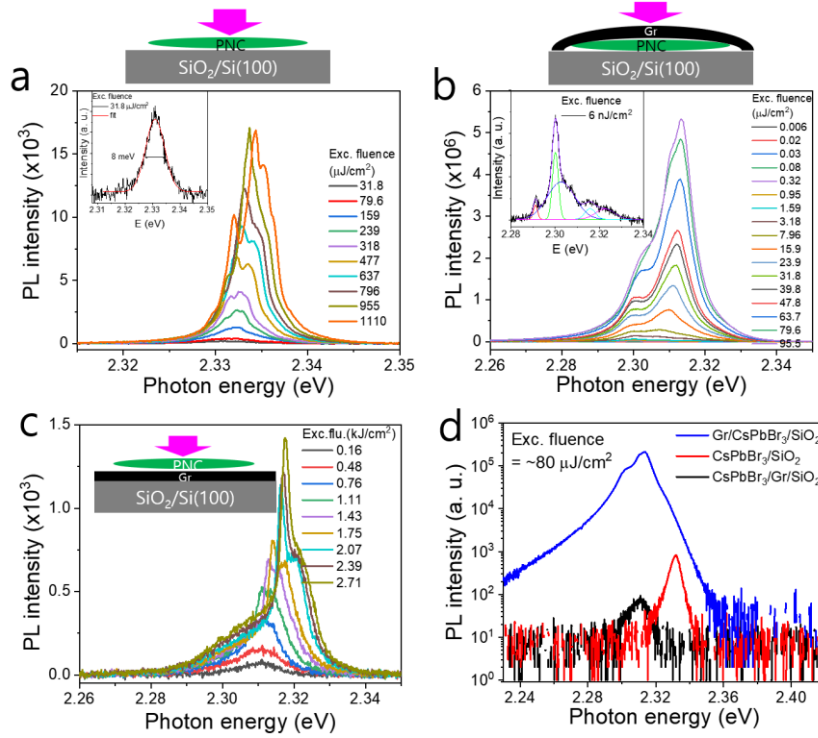


Fig. 2. (a) Power-dependent μ PL spectra measured for the bare CsPbBr₃ QD cluster. Inset depicts the PL spectrum and fit (red) at the lowest excitation fluence. (b) Power-dependent μ PL spectra taken for a Gr-coated CsPbBr₃ heterostructure cluster. Inset depicts the PL spectrum and fit at the lowest excitation fluence. (c) The power-dependent μ PL spectra of the CsPbBr₃/Gr structure. (d) Comparison of PL spectra for Gr/CsPbBr₃ and CsPbBr₃ structures at similar excitation fluence ($\sim 80 \mu\text{J}/\text{cm}^2$). For the CsPbBr₃/Gr, the excitation fluence is $\sim 160 \mu\text{J}/\text{cm}^2$. Schematics above each graph illustrate the corresponding sample structure.

The model structure is described in the method section and is illustrated (Fig. 3a and Fig. S2). According to the DFT calculation results, the CsPbBr₃/Gr interface is stabilized through weak van der Waals interaction with an interlayer distance of 3.4 \AA and binding energy of -0.03 eV per carbon atom (Eq. S1 in supporting information). The ground state electronic band structure of the CsPbBr₃/Gr/SiO₂ heterostructure, including a perovskite symmetry slab with PbBr₂ termination, is depicted in Fig. 3a.

The CsPbBr₃ layer shows a direct band gap of 1.9 eV located at the Γ point. In addition, upon forming CsPbBr₃/Gr interface, electrons transfer from the CsPbBr₃ to the graphene, indicating the n-doped character of graphene as evidenced by the Dirac point appearing below the Fermi level. Moreover, the Fermi level is strongly pinned to the perovskite's valence band maximum (VBM). Therefore, under the illumination of the perovskite light absorber, electrons will readily transfer from the graphene layer to photo-generated empty states in the perovskite valence band. Consequently, the radiative recombination of photo-excited electron-hole pairs in perovskite will be suppressed, leading to PL quenching in the CsPbBr₃/Gr/SiO₂ system, which agrees with previous reports [4,19,20]. The Fermi level pinning at the perovskite VBM is confirmed to appear when the PbBr₂-terminated surface is in contact with Gr/SiO₂, being independent of the terminal type of the opposite side (Figs. S3a-c).

We also modeled the Gr/CsPbBr₃/SiO₂ heterostructure (Fig. 3b and Fig. S2) to determine the reason for the PL intensity enhancement. Like the CsPbBr₃/Gr/SiO₂ heterostructure, the interfacial interaction at the Gr/CsPbBr₃ junction is of van der Waals type with an interlayer distance of 3.3 Å and a binding energy of -0.03 eV per carbon atom (Eq. S2 in supporting information). The ground state electronic band structure of the Gr/CsPbBr₃/SiO₂ heterostructure is shown in Fig. 3b. The CsPbBr₃ layer exhibits a direct band gap of 1.80 eV at the Γ point, which is slightly reduced compared with CsPbBr₃/Gr/SiO₃ heterostructure, and Gr's Dirac cone is located between the Γ and X points. Interacting with the SiO₂ interface dipole increases the CsPbBr₃ work function, leading to a downward shift of its VBM and CBM.

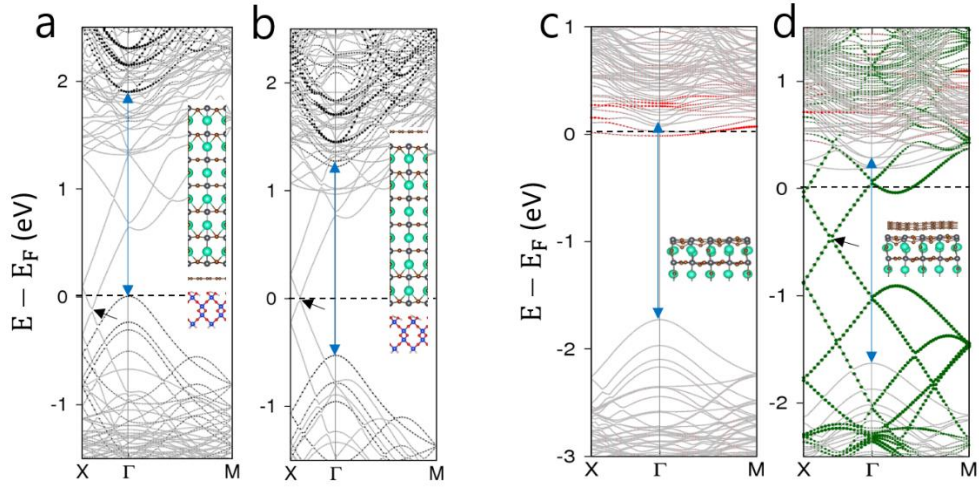


Fig. 3. Calculated band structure of (a) CsPbBr₃/Gr/SiO₂ (inset: side view along [100] of the model heterostructure). (b) Gr/CsPbBr₃/SiO₂. For easier recognition of the CsPbBr₃ band edges, the Pb bulk atom's 6p orbital contribution is shown by black circles. (c) CsPbBr₃ with a V_{Br} surface defect (inset: side view along [100] of the top 4 atomic layers of the model structure). (d) a defected CsPbBr₃/Gr interface (inset: side view along the [100] interface model structure with a perovskite top 4 atomic layers). Red circles show the contribution of the under-coordinated Pb atoms, and the carbon p_z orbital contribution is indicated by green circles. In all band structures, the electronic transition between the CsPbBr₃ band edges is indicated by the blue arrow. Gr's Dirac point is indicated by the black arrow in (a), (b), and (d). Atomic color scheme: Cs (green), Pb (gray), Br (brown), Si (blue), O (red), H (pink), C (brown).

This, in turn, enhances the interfacial electrostatic potential barrier for charge transfer at the Gr/CsPbBr₃ interface which is evident by comparing the position of the perovskite's VBM and CBM relative to the graphene Dirac point (Fig. 3b). Furthermore, following the downshift of the perovskite energy levels, the interfacial orbital coupling at the Gr/CsPbBr₃ interface is suppressed. Therefore, the formation of the

Gr/CsPbBr₃/SiO₂ heterostructure does not result in charge transfer at the Gr/perovskite interface in its ground state, even for the other termination types of the perovskite layer (Figs. S3d-f). Under illumination, the interfacial electrostatic potential barriers are high enough to prevent carrier leakage from the perovskite layer to graphene, which enhances radiative recombination compared to CsPbBr₃/Gr/SiO₂ heterostructure.

Another possibility for explaining the PL enhancement could be associated with a surface stabilization effect via defect passivation, as we have shown in our previous work on passivation effect giving rise to significant PL enhancement [25]. We explored the structural and electronic properties of a defected CsPbBr₃ layer with and without graphene on its surface. Since a Br vacancy (V_{Br}) is reported to be the predominant defect in CsPbBr₃ perovskites [23,45], we introduced a V_{Br} into a PbBr₂-terminated CsPbBr₃ (001) surface (Fig. S4). The optimized geometry for the defected interface (Inset in Fig. 3d) indicates structural distortions in the perovskite top layers caused by V_{Br} . Gr is physisorbed on the perovskite surface with a binding energy of -0.03 eV per carbon atom (Eq. S3 in supporting information). We should note that the graphene deformation is an artifact of our model supercell. As shown in Fig. 3c, the V_{Br} generates a localized trap state close to the CsPbBr₃ conduction band minimum (CBM), which can act as a center for nonradiative recombination and suppress the PL intensity. However, after covering defected CsPbBr₃ with graphene, carbon p_z states hybridized with Pb dangling bond states and shifted them upward to the perovskite conduction band (Fig. 3d). Therefore, the Gr adsorption on the defected CsPbBr₃ surface eliminates nonradiative recombination centers leading to PL enhancement in the Gr/CsPbBr₃/SiO₂

system. It should be noted that upon passivation of the V_{Br} defect, the Gr is n-doped (Fig. 3d) with a charge density of 10^{13} cm^{-2} (Eq. S4 in supporting information) [46]. Similar results are obtained for the Gr/CsPbBr₃ interface consisting of the perovskite with a CsBr termination (Figs. S4 and S5).

Enhanced PL emission due to the resonant coupling between surface plasmon (SP) modes in a metallic layer and excitons in a semiconductor has been reported [31,42,47-51]. Considering the semi-metallic nature of graphene, the significant PL enhancement of the Gr/CsPbBr₃/SiO₂ heterosystem could be understood in terms of the resonant excitation of graphene plasmon modes [29-31,50]. The perovskite's photo-generated excitons can induce a resonant plasmon mode in the graphene layer. However, because of the considerable momentum mismatch between the Gr's plasmon and photons in free space, a lateral modulation periodicity on the graphene [29,30] or its substrate [31] is required to resolve the momentum mismatch and transform the excited plasmon mode to the light emission. The dispersion relation of the graphene plasmon in the random phase approximation is

$$\omega(\mathbf{q}) = \left[\frac{n_e e^2}{\epsilon_0 (1+\epsilon_b) m^*} |\mathbf{q}| + \frac{3}{4} v_F^2 \mathbf{q}^2 \right]^{1/2} \quad (1)$$

where q is the in-plane wave number, n_e is the electron density, ϵ_0 is the vacuum permittivity, ϵ_b is the substrate static dielectric constant, m^* is electron effective mass in Gr, and v_F is its Fermi velocity [31,51,52]. We supposed that the graphene plasmon could be resonantly excited at perovskite band gap energy of 2.3 eV and calculated the in-plane momentum q from our calculated $n_e = 10^{13} \text{ cm}^{-2}$, using $\epsilon_b = 18.6$ for the CsPbBr₃ substrate [21,53], $m^* = 0.077 m_e$ where m_e is the free electron mass, and $v_F =$

1.12×10^6 m/s [31]. We obtained $q = 2\pi/1.8 \text{ nm}^{-1}$, indicating a lateral modulation periodicity of $a = 1.8 \text{ nm}$ at the Gr/CsPbBr₃ interface would be required to extract light from the Gr's plasmon. Due to the V_{Br} defects, the surface structure of the CsPbBr₃ is distorted and not perfectly flat, resulting in interface corrugations on the order of a few nm. While it may not be feasible to measure $a = 1.8 \text{ nm}$ experimentally, this value is consistent with the lateral distance of 1.68 nm between V_{Br} surface defects in our model structure. Thus, the resonant activation of a Gr plasmon at the perovskite band gap, and its conversion to photons via interaction with interface surface corrugations, explains the observed PL enhancement for the Gr/CsPbBr₃/SiO₂ heterostructure. A schematic diagram of the explained mechanism is depicted in Fig. 4a. We also conducted TRPL measurements on bare and Gr-covered CsPbBr₃ NCs to understand the dynamics of photoexcited carriers. The PL signals of both samples show a biexponential decay over time as presented in Fig. 4b. The fast decay component of bare CsPbBr₃ NCs is 0.61 ns, which reduced to 0.5 ns for Gr-covered CsPbBr₃ NCs, originating from the direct recombination of photoexcited charge carriers [54,55] in both samples. On the other hand, the slow decay component indicates the presence of a secondary source for PL emission, attributed to shallow trap-assisted recombination (V_{Br} in our case) [54]. The slow decay component for bare CsPbBr₃ NCs is 3.26 ns which reduces to 2.96 ns for the Gr-covered sample, confirming the decrease of surface defect states by Gr covering.

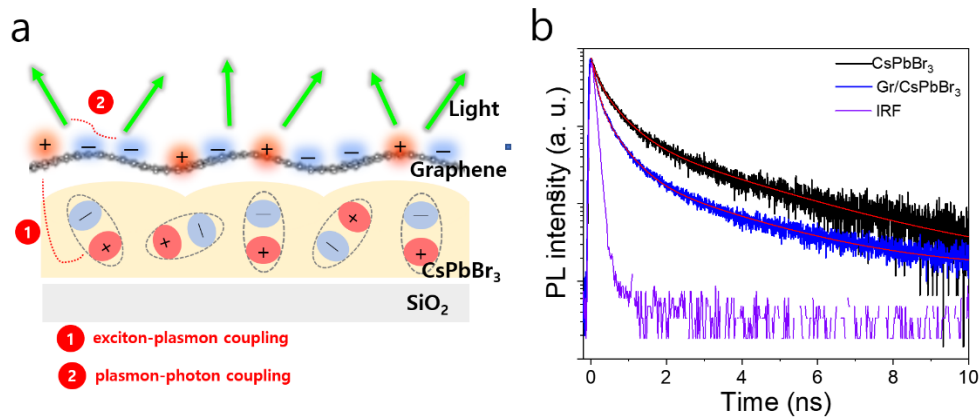


Fig. 4. (a) Schematic diagram of the emission from exciton-plasmon and plasmon-photon coupling. (b) Time-resolved PL comparison for bare CsPbBr₃ QDs (uncoated) and Gr-covered QD clusters. The data of bare CsPbBr₃ and Gr-covered CsPbBr₃ are fitted with biexponential decays and the decay times are 0.61 ns and 0.5 ns for faster components and 2.96 ns and 3.26 ns for slow components, respectively. The TRPL measurement accuracy is 120 ps.

4. Conclusions

In summary, we have demonstrated the optical characterization of bare CsPbBr₃ QDs and graphene-covered CsPbBr₃ QDs by micro-photoluminescence measurements and density functional theory calculations. Compared with bare CsPbBr₃ QDs, the PL intensity of the Gr-covered CsPbBr₃ QDs is dramatically enhanced by three orders of magnitude. The DFT calculation results showed that contacting Gr on the top side of CsPbBr₃ causes the Dirac point to appear at the center of CsPbBr₃ energy gap, in contrast to the Fermi level pinning behavior to the valence band edge reported for bottom side contact as in CsPbBr₃/Gr/SiO₂. Thus, carrier leakage is prevented for the Gr-covered CsPbBr₃ with a high radiative recombination rate. In addition, the

perovskite's surface defects are passivated via the graphene covering, suppressing the nonradiative recombination of photo-generated charge carriers compared to uncovered perovskite QDs. Furthermore, resonant excitation of graphene plasmon by the perovskite's photo-generated excitons, followed by its conversion to photons through interaction with Gr/CsPbBr₃ interface corrugations, substantially enhances the photoluminescence from Gr/CsPbBr₃/SiO₂ heterosystem. Our experimental and theoretical investigations show the significant role of graphene covering for dramatic PL enhancement of CsPbBr₃, which can be implemented for developing super bright light-emitting diodes.

References

- [1] M. Liu, M. B. Johnston, H. J. Snaith, Efficient planar heterojunction perovskite solar cells by vapour deposition, *Nature* 501 (2013) 395–398.
- [2] M. A. Green, A. Ho-Baillie, H. J. Snaith, The emergence of perovskite solar cells, *Nat. Photo.* 8 (2014) 506–514.
- [3] H. Cho, S.-H. Jeong, M.-H. Park, Y.-H. Kim, C. Wolf, C.-L. Lee, J. H. Heo, A. Sadhanala, N. Myoung, S. Too, S. H. Im, R. H. Friend, T.-W. Lee, Overcoming the electroluminescence efficiency limitations of perovskite light-emitting diodes. *Science* 350 (2015) 1222.
- [4] D.-H. Kwak, D.-H. Lim, H.-S. Ra, P. R. Ra, J.-S. Lee, High performance hybrid graphene–CsPbBr₃₋₁I_x, *RSC Adv.* 6 (2016) 65252.
- [5] J. Liang, C. Wang, Y. Wang, Z. Xu, Z. Lu, Y. Ma, H. Zhu, Y. Hu, C. Xiao, X. Yi, G.

- Zhu, H. Lv, L. Ma, T. Chen, Z. Tie, Z. Jin, J. Liu, All-inorganic perovskite solar cells, *J. American Chem. Soc.* 138 (2016) 15829–15832.
- [6] M. Kulbak, S. Gupta, N. Kedem, I. Levine, T. Bendikov, G. Hodes, D. Cahen, Cesium enhances long-term stability of lead bromide perovskite-based solar cells, *J. Phys. Chem. Lett.* 7 (2016) 167–172.
- [7] P. Wang, X. Zhang, Y. Zhou, Q. Jiang, Q. Ye, Z. Chu, X. Li, X. Yang, Z. Yin, J. You, Solvent-controlled growth of inorganic perovskite films in dry environment for efficient and stable solar cells, *Nat. Commun.* 9 (2018) 2225.
- [8] A. Swarnkar, R. Chulliyil, V. K. Ravi, M. Irfanullah, A. Chowdhury, A. Nag, Colloidal CsPbBr₃ perovskite nanocrystals: Luminescence beyond traditional quantum dots, *Ang. Chem. – Internat. Ed.* 54 (2015) 15424–15428.
- [9] J. Kang, L. W. Wang, W. High defect tolerance in lead halide perovskite CsPbBr₃, *J. Phys. Chem. Lett.* 8 (2017) 489–493.
- [10] G. Raino, G. Nedelcu, L. Protesescu, M. I. Bodnarchuk, M. V. Kovalenko, R. F. Mahrt, T. Stöferle, Single cesium lead halide perovskite nanocrystals at low temperature: Fast single-photon emission, reduced blinking, and exciton fine structure, *ACS Nano* 10 (2016) 2485–2490.
- [11] C. C. Stoumpos, C. D. Malliakas, J. A. Peters, Z. Liu, M. Sebastian, J. Im, T. C. Chasapis, A. C. Wibowo, D. Y. Chung, A. J. Freeman, B. W. Wessels, M. G. Kanatzidis, Crystal Growth of the Perovskite Semiconductor CsPbBr₃: A new material for high-energy radiation detection, *Cryst. Growth and Design* 13 (2013) 2722–2727.

- [12] G. Ying, A. Jana, V. Osokin, T. Farrow, R. A. Taylor, Y. Park, Highly efficient photoluminescence and lasing from hydroxide coated fully inorganic perovskite micro/nano-rods, *Adv. Opt. Mater.* 8 (2020) 2001235.
- [13] S. Yakunin, L. Protesescu, F. Krieg, M. I. Bodnarchuk, G. Nedelcu, M. Humer, G. De Luca, M. Fiebig, W. Heiss, M. V. Kovalenko, Low-threshold amplified spontaneous emission and lasing from colloidal nanocrystals of caesium lead halide perovskites, *Nat. Commun.* 6 (2015) 8056.
- [14] W. Du, S. Zhang, J. Shi, J. Chen, Z. Wu, Y. Mi, Z. Liu, Y. Li, X. Sui, R. Wang, X. Qiu, T. Wu, Y. Xiao, Q. Zhang, X. Liu, Strong exciton–photon coupling and lasing behavior in all- inorganic CsPbBr₃ micro/nanowire Fabry-Pérot cavity, *ACS Phot.* 5 (2018) 2051–2059.
- [15] M. A. Becker, R. Vaxenburg, G. Nedelcu, P. C. Sercel, A. Shabaev, M. J. Mehl, J. G. Michopoulos, S. G. Lambrakos, N. Bernstein, J. L. Lyons, T. Stöferle, R. F. Mahrt, M. V. Kovalenko, D. J. Norris, G. Rainò, A. L. Efros, Bright triplet excitons in caesium lead halide perovskites, *Nature* 553 (2018) 189–193.
- [16] G. Rainò, M. A. Becker, M. I. Bodnarchuk, R. F. Mahrt, M. V. Kovalenko, T. Stöferle, Superfluorescence from lead halide perovskite quantum dot superlattices, *Nature* 563 (2018) 671–675.
- [17] A. K. Geim, K. S. Novoselov, The rise of graphene progress, *Nat. Mater.* 6 (2007) 183–191.
- [18] R. R. Nair, P. Blake, A. N. Grigorenko, K. S. Novoselov, T. J. Booth, T. Stauber, N. M. R. Peres, A. K. Geim, Fine structure constant defines visual transparency of

- graphene, *Science* 320 (2008) 1308.
- [19] J. Yun, H. Fan, Y. Zhang, R. Huang, Y. Ren, M. Guo, H. An, P. Kang, H. Guo, Enhanced optical absorption and interfacial carrier separation of CsPbBr₃/graphene heterostructure: Experimental and theoretical insights, *ACS Appl. Mater. & Inter.* 12 (2020) 3086–3095.
- [20] Y. Lee, J. Kwon, E. Hwang, C.-H. Ra, W. J. Yoo, J.-H. Ahn, J. H. Park, J. H. Cho, High-performance perovskite graphene hybrid photodetector, *Adv. Mater.* 27 (2015) 41–46.
- [21] J. Kang, J. Li, S. H. Wei, Atomic-scale understanding on the physics and control of intrinsic point defects in lead halide perovskites, *Appl. Phys. Rev.* 8 (2021) 031302.
- [22] G. H. Ahmed, J. K. El-Demellawi, J. Yin, J. Pan, D. B. Velusamy, M. N. Hedhili, E. Alarousu, O. M. Bakr, H. N. Alshareef, O. F. Mohammed, Photoluminescence enhancement in CsPbCl₃ perovskite nanocrystals by simultaneous dual-surface passivation, *ACS Energy Lett.* 3 (2018) 2301–2307.
- [23] J. Pan, X. Li, X. Gong, J. Yin, D. Zhou, L. Sinatra, R. Huang, J. Liu, J. Chen, I. Dursun, A. M. El-Zohry, M. I. Saidaminov, H.-T. Sun, O. F. Mohammed, C. Ye, E. H. Sargent, O. M. Bakr, Halogen vacancies enable ligand-assisted self-assembly of perovskite quantum dots into nanowires, *Angew. Chem. Int. Ed.* 58 (2019) 16077–16081.
- [24] J. Meiss, A. Merten, M. Hein, C. Schuenemann, S. Schäfer, M. Tietze, C. Uhrich, M. Pfeiffer, K. Leo, M. Riede, Fluorinated zinc phthalocyanine as donor for

- efficient vacuum-deposited organic solar cells, *Adv. Funct. Mater.* 22 (2012) 405–414.
- [25] Y. Park, A. Jana, C. W. Myung, T. Yoon, G. Lee, C. C. Kocher, G. Ying, V. Osokin, R. A. Taylor, K. S. Kim, Enhanced photoluminescence quantum yield of MAPbBr₃ nanocrystals by passivation using graphene, *Nano Research* 13 (2020) 932–938.
- [26] D. Y. Lei, J. Li, H. C. Ong, Tunable surface plasmon mediated emission from semiconductors by using metal alloys, *Appl. Phys. Lett.* 91 (2007) 021112.
- [27] J. Li, H. C. Ong, Temperature dependence of surface plasmon mediated emission from metal-capped ZnO films, *Appl. Phys. Lett.* 92 (2008) 121107.
- [28] K. Okamoto, I. Niki, A. Shvartser, Y. Narukawa, T. Mukai, A. Scherer, Surface-plasmon-enhanced light emitters based on InGaN quantum wells, *Nat. Mater.* 3 (2004) 601-605.
- [29] Y. L. Chen, Y. J. Ma, D. D. Chen, W. Q. Wang, K. Ding, Q. Wu, Y. L. Fan, X. J. Yang, Z. Y. Zhong, F. Xu, Z. M. Jiang, Effect of graphene on photoluminescence properties of graphene/GeSi quantum dot hybrid structures, *Appl. Phys. Lett.* 105 (2014) 021104.
- [30] M. Farhat, S. Guenneau, H. Bağcı, Exciting graphene surface plasmon polaritons through light and sound interplay, *Phys. Rev. Lett.* 111 (2013) 237404.
- [31] S. W. Hwang, D. H. Shin, C. O. Kim, S. H. Hong, M. C. Kim, J. Kim, K. Y. Lim, S. Kim, S. H. Choi, K. J. Ahn, G. Kim, S. H. Sim, B. H. Hong, Plasmon-enhanced ultraviolet photoluminescence from hybrid structures of graphene/ZnO films, *Phys.*

- Rev. Lett. 105 (2010) 127403.
- [32] Y. Chen, Z. Dong, B. Wang, Z. Jiang, X. Wang, The photoelectric response of the graphene/GeSi QDs hybrid structure, *Nanotechnology* 29 (2018) 504005.
- [33] G. Kresse, J. Furthmüller, Efficiency of Ab-initio total energy calculations for metals and semiconductors using a plane-wave basis set, *Comput. Mater. Sci.* 6 (1996) 15.
- [34] J. P. Perdew, K. Burke, M. Ernzerhof, Generalized gradient approximation made simple, *Phys. Rev. Lett.* 77 (1996) 3865.
- [35] A. Tkatchenko, M. Scheffler, Accurate molecular van Der Waals interactions from ground-state electron density and free-atom reference data, *Phys. Rev. Lett.* 102 (2009) 073005.
- [36] H. M. Ghaithan, Z. A. Alahmed, S. M. H. Qaid, M. Hezam, A. S. Aldwayyan, Density functional study of cubic, tetragonal, and orthorhombic CsPbBr₃ perovskite, *ACS Omega* 5 (2020) 7468.
- [37] J. Yun, H. Fan, Y. Zhang, R. Huang, Y. Ren, M. Guo, H. An, P. Kang, H. Guo, Enhanced optical absorption and interfacial carrier separation of CsPbBr₃/graphene heterostructure: experimental and theoretical insights, *ACS Appl. Mater. & Inter.* 12 (2020) 3086.
- [38] J. A. Castañeda, G. Nagamine, E. Yassitepe, L. G. Bonato, O. Voznyy, S. Hoogland, A. F. Nogueira, E. H. Sargent, C. H. B. Cruz, L. A. Padilha, Efficient biexciton interaction in perovskite quantum dots under weak and strong confinement, *ACS Nano* 10 (2016) 8603–8609.

- [39] F. Krieg, S. T. Ochsenbein, S. Yakunin, S. Ten Brinck, P. Aellen, A. Süess, B. Clerc, D. Guggisberg, O. Nazarenko, Y. Shynkarenko, S. Kumar, C. J. Shih, I. Infante, M. V. Kovalenko, Colloidal CsPbX₃ (X = Cl, Br, I) nanocrystals 2.0: Zwitterionic capping ligands for improved durability and stability, *ACS Energy Lett.* 3 (2018) 641–646.
- [40] Y. Wang, X. Li, J. Song, L. Xiao, H. Zeng, H. Sun, All-inorganic colloidal perovskite quantum dots: A new class of lasing materials with favorable characteristics, *Adv. Mater.* 27 (2015) 7101–7108.
- [41] J. Song, J. Li, X. Li, L. Xu, Y. Dong, H. Zeng, Quantum dot light-emitting diodes based on inorganic perovskite cesium lead halides (CsPbX₃), *Adv. Mater.* 27 (2015) 7162–7167.
- [42] W. Zhao, Z. Wen, Q. Xu, Z. Zhou, S. Li, S. Fang, T. Chen, L. Sun, X. Wang, Y. Liu, Y. Sun, Y. W. Tan, N. Dai, J. Hao, Remarkable photoluminescence enhancement of CsPbBr₃ perovskite quantum dots assisted by metallic thin films, *Nanophoto.* 10 (2021) 2257–2264.
- [43] H. Utzat, W. Sun, A. E. K. Kaplan, F. Krieg, M. Ginterseder, B. Spokoyny, N. D. Klein, K. E. Shulenberger, C. F. Perkinson, M. V. Kovalenko, M. G. Bawendi, Coherent single-photon emission from colloidal lead halide perovskite quantum dots, *Science* 363 (2019) 1068–1072.
- [44] Q. Xiong, S. Huang, J. Du, X. Tang, F. Zeng, Z. Liu, Z. Zhang, T. Shi, J. Yang, D. Wu, H. Lin, Z. Luo, Y. Leng, Surface ligand engineering for CsPbBr₃ quantum dots aiming at aggregation suppression and amplified spontaneous emission

- improvement, *Adv. Opt. Mater.* 8 (2020) 2000977.
- [45] J. Yin, H. Yang, K. Song, A. M. El-Zohry, Y. Han, O. M. Bakr, J. L. Brédas, O. F. Mohammed, Point defects and green emission in zero-dimensional perovskites, *J. Phys. Chem. Lett.* 9 (2018) 5490–5495.
- [46] F. Joucken, Y. Tison, J. Lagoute, J. Dumont, D. Cabosart, B. Zheng, V. Repain, C. Chacon, Y. Girard, A. R. Botello-Mendez, S. Rousset, R. Sporken, J. C. Charlier, L. Henrard, Localized state and charge transfer in nitrogen-doped graphene, *Phys. Rev. B.* 85 (2012) 161408(R).
- [47] J. Li, S. K. Cushing, F. Meng, T. R. Senty, A. D. Bristow, N. Wu, Plasmon-induced resonance energy transfer for solar energy conversion, *Nat. Photo.* 9 (2015) 601–607.
- [48] K. Yao, S. Li, Z. Liu, Y. Ying, P. Dvořák, L. Fei, T. Šikola, H. Huang, P. Nordlander, A. K. Y. Jen, D. Lei, Plasmon-induced trap filling at grain boundaries in perovskite solar cells, *Light: Sci. Appl.* 10 (2021) 219.
- [49] X. Huang, H. Li, C. Zhang, S. Tan, Z. Chen, L. Chen, Z. Lu, X. Wang, M. Xiao, Efficient plasmon-hot electron conversion in Ag–CsPbBr₃ hybrid nanocrystals, *Nat. Commun.* 10 (2019) 1163.
- [50] K. Okamoto, M. Funato, Y. Kawakami, K. Tamada, High-efficiency light emission by means of exciton–surface-plasmon coupling, *J. Photochem. Photobio. C: Photochem. Rev.* 32 (2017) 58–77.
- [51] Y. Liu, R. F. Willis, K. V. Emtsev, T. Seyller, Plasmon dispersion and damping in electrically isolated two-dimensional charge Sheets, *Phys. Rev. B.* 78 (2008)

201403(R).

- [52] Y. Liu, R. F. Willis, Plasmon-phonon strongly coupled mode in epitaxial graphene, *Phys. Rev. B.* 81 (2010) 081406(R).
- [53] M. R. Filip, J. B. Haber, J. B. Neaton, Phonon screening of excitons in semiconductors: halide perovskites and beyond, *Phys. Rev. Lett.* 127 (2021) 67401.
- [54] M. Seitz, M. Melendez, N. Alcázar-Cano, D. N. Congreve, R. Delgado-Buscalioni, F. Prins, Mapping the trap-state landscape in 2D metal-halide perovskites using transient photoluminescence microscopy, *Adv. Opt. Mater.* 9 (2021) 2001875.
- [55] J.-H. Park, Y. Reo, J.-H. Jung, T. Kim, T. Park, Y.-Y. Noh, C.-J. Kim, Reduction of hole carriers by van der Waals contact for enhanced photoluminescence quantum yield in two-dimensional tin halide perovskite, *ACS Energy Lett.* 8 (2023) 3536.

Supplementary Information for

Surface plasmon-mediated photoluminescence boost in graphene-covered CsPbBr₃ quantum dots

Youngsin Park ^a, Elham Oleiki ^a, Guanhua Ying ^b, Atanu Jana ^c, Mutibah Alanazi ^b, Vitaly Osokin ^b, Sangeun Cho ^c, Robert A. Taylor ^{b,*}, Geunsik Lee ^{a,*}

^a Department of Chemistry, College of Natural Science, Ulsan National Institute of Science and Technology, Ulsan 44919, Korea

^b Clarendon Laboratory, Department of Physics, University of Oxford, Parks Road, Oxford OX1 3PU, UK

^c System Semiconductor Science, Dongguk University, Seoul 04620, Korea

†These authors are contributed equally to this work

*Correspondence authors. E-mail: robert.taylor@physics.ox.ac.uk, gslee@unist.ac.kr

Density functional theory calculations

To model the CsPbBr₃ surface with V_{Br} defects, we used the ideal CsPbBr₃/Gr supercell, and repeated it twice along the [010] direction (Figure S4), and introduced one surface Br vacancy per each 1×2 supercell. Our defective model of CsPbBr₃ slab corresponds to the surface defect concentration of 10¹³ cm⁻², comparable to the experimental value [1,2]. Atomic positions of the Gr layer and four top atomic layers of the CsPbBr₃ surface were optimized. We performed PBE electronic structure calculations on a 4×4×1 *k*-point mesh by setting energy convergence criteria and kinetic energy cutoff 10⁻⁴ and 400 eV, respectively. Our calculated direct band gap for cubic bulk structure is 1.53 eV which is consistent with other theoretical reports [3]; however, it underestimates the experimental value of 2.22 eV [4]. To get a better agreement with the experimental band gap, GW+SOC or HSE+SOC methods should be implemented [3,5]; though, considering the high number of atoms in our supercells (more than 300), employing this level of calculation was not plausible. Nonetheless, the main characteristics of the conduction and valance bands of CsPbBr₃ are maintained using the PBE method [6]. In addition, because of the quantum confinement effect, the band gap of the CsPbBr₃ layer increased to 1.85 eV which is closer to the experimental value. Therefore, we performed all the electronic structure calculations using the PBE method.

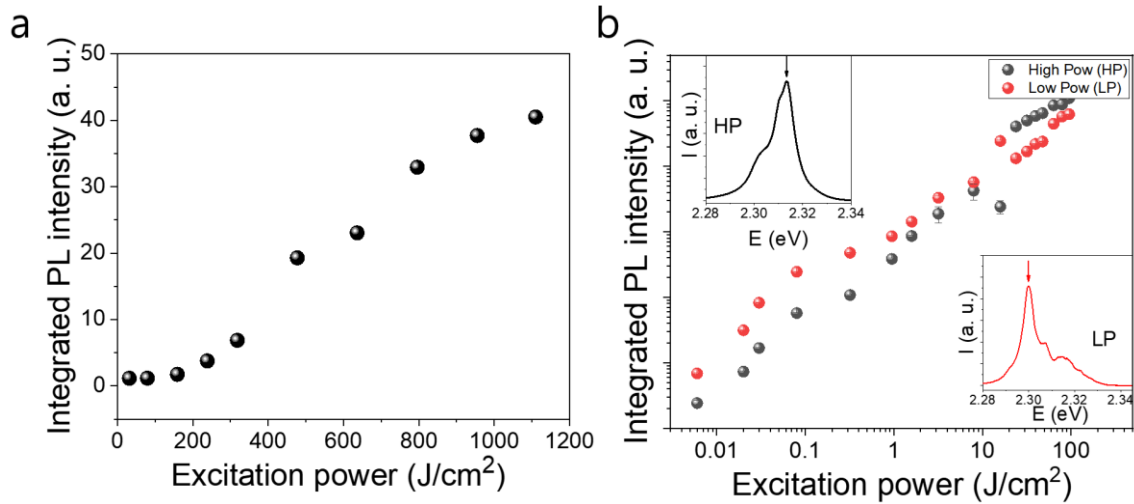


Fig. S1. (a) Integrated PL intensity of the bare CsPbBr₃ QDs red dot marked peak in Fig. 2a. (b) Integrated PL intensity of the Gr-covered CsPbBr₃ QDs at the main peaks of the low and high excitation power. Here, LP and HP mean the low excitation power and high excitation power, respectively.

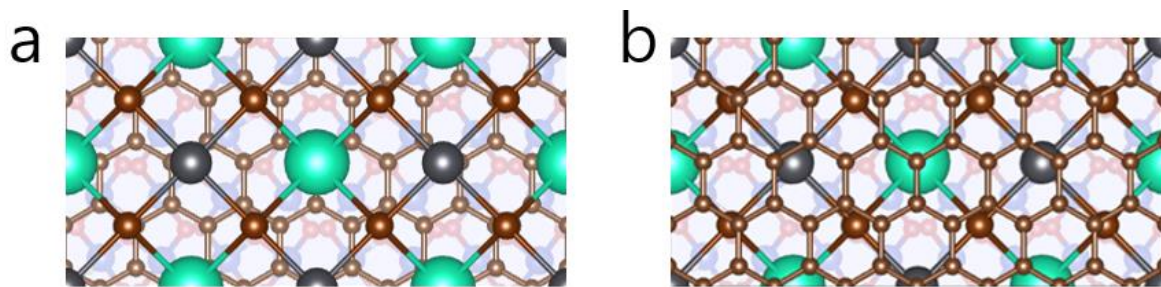


Fig. S2. Top view of $2 \times \sqrt{2} \times \sqrt{2}$ surface supercell of (a) CsPbBr₃/Gr/SiO₂, and (b) Gr/CsPbBr₃/SiO₂. Atomic color scheme: Cs (green), Pb (gray), Br (brown), Si (blue), O (red), H (pink), C (brown).

Electronic band structure of the three-layered heterostructure considering CsPbBr₃ layer with CsBr and PbBr₂ terminations

Considering both CsBr and PbBr₂ surface terminations of the perovskite layer, we calculated the ground state electronic band structure of four CsPbBr₃/Gr/SiO₂ (Figures S3a-c Figure 3a) and four Gr/CsPbBr₃/SiO₂ model heterostructures (Figures 3d-e and Figure 3b) to screen all possible interfacial interactions and their impact on the electronic structure. Among all CsPbBr₃/Gr/SiO₂ model heterostructures, the model including a CsPbBr₃ (001) slab with PbBr₂

top and bottom terminations (Figure 3a) showed considerable charge transfer at the Gr/CsPbBr₃ interface. However, none of the Gr/CsPbBr₃/SiO₂ model heterostructures showed interfacial charge transfer at the CsPbBr₃/Gr interface.

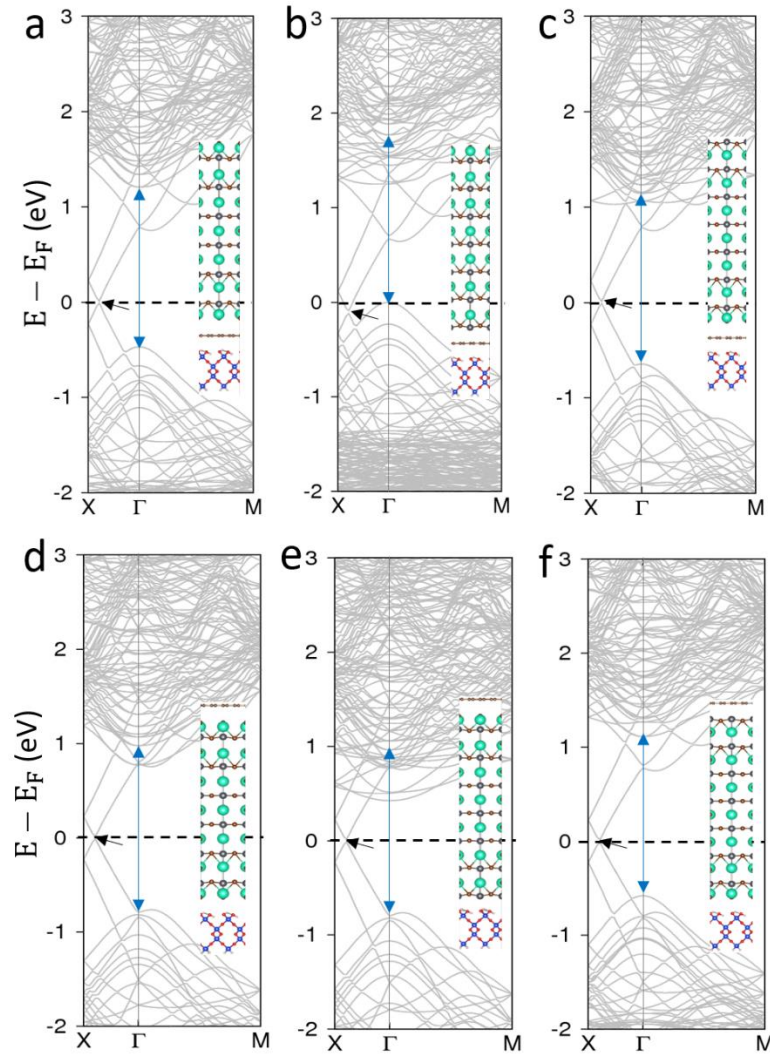


Fig. S3. Calculated electronic band structure of (a)(b)(c) CsPbBr₃/Gr/SiO₂, and (d)(e)(f) Gr/CsPbBr₃/SiO₂ with different perovskite surface terminations. The electronic transition between the CsPbBr₃ band edges is indicated by the blue arrow, and graphene's Dirac point is mentioned by the black arrow. All side views in the insets are along [100]. Atomic color scheme: Cs (green), Pb (gray), Br (brown), Si (blue), O (red), H (pink), C (brown).

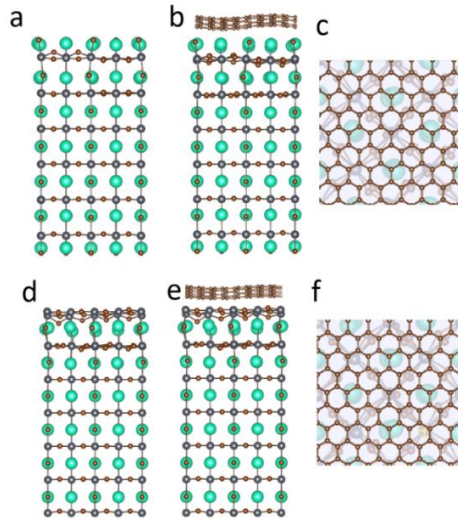


Fig. S4. Side view along $[100]$ of (a) CsBr terminated (001) CsPbBr₃ slab with V_{Br} surface defect and (b) its interface with Gr. (c) Top view of (b). (d) PbBr₂ terminated (001) CsPbBr₃ slab with V_{Br} surface defect and (e) its interface with Gr. (f) Top view of (e). Atomic color scheme: Cs (green), Pb (gray), Br (brown), Si (blue), O (red), H (pink), C (brown).

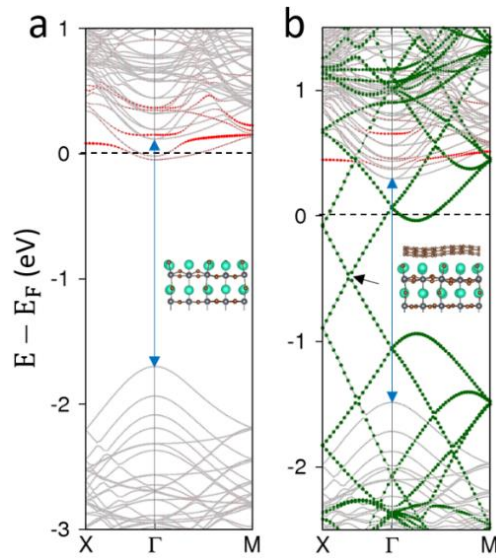


Fig. S5. Calculated electronic band structure of (a) CsBr terminated (001) CsPbBr₃ slab with V_{Br} surface defect (inset: side view along $[100]$ of the top 4 atomic layers of model structure). (b) defected CsPbBr₃/Gr interface (inset: side view along $[100]$ of interface model structure with perovskite top 4 atomic layers). Red circles show the contribution of under-coordinated Pb atom, and carbon p_z orbital contribution is indicated by green circles. In all band structures, CsPbBr₃ band edges are indicated by arrows. Atomic color scheme: Cs (green), Pb (gray), Br (brown), Si (blue), O (red), H (pink), C (brown).

Interlayer binding energy

Equations S1 to S3 define the binding energy of Gr and perovskite layer in CsPbBr₃/Gr/SiO₂, Gr/CsPbBr₃/SiO₂, and Gr/CsPbBr₃ heterostructure, respectively:

$$E_B = E(\text{CsPbBr}_3/\text{Gr}/\text{SiO}_2) - E(\text{Gr}/\text{SiO}_2) - E(\text{CsPbBr}_3) \quad (\text{Eq. S1})$$

$$E_B = E(\text{Gr}/\text{CsPbBr}_3/\text{SiO}_2) - E(\text{Gr}) - E(\text{CsPbBr}_3/\text{SiO}_2) \quad (\text{Eq. S2})$$

$$E_B = E(\text{Gr}/\text{CsPbBr}_3) - E(\text{CsPbBr}_3) - E(\text{Gr}) \quad (\text{Eq. S3})$$

where $E(\text{CsPbBr}_3/\text{Gr}/\text{SiO}_2)$ is the total energy of CsPbBr₃/Gr/SiO₂ heterostructure, $E(\text{Gr}/\text{SiO}_2)$ is the total energy of Gr/SiO₂ heterostructure, $E(\text{CsPbBr}_3)$ the total energy of isolated CsPbBr₃, $E(\text{Gr}/\text{CsPbBr}_3/\text{SiO}_2)$ is the total energy of Gr/CsPbBr₃/SiO₂ system, $E(\text{Gr})$ is the total energy of isolated Gr layer, and $E(\text{Gr}/\text{CsPbBr}_3)$ is the total energy of Gr/CsPbBr₃ heterostructure. According to these definitions, negative (positive) value of E_B suggests a stable (unstable) interface.

Electron density in the graphene layer

Equation S4 relates the Dirac energy in electronic band structure to electron density in the Gr layer:

$$n_e = \frac{E_D^2}{\pi (\hbar v_F)^2} \quad (\text{Eq. S4})$$

where v_F is Fermi velocity. For $E_D = 0.5$ eV (from electronic band structure of Gr/defected-CsPbBr₃ interface (Figure 3d)) and $v_F = 1.12 \times 10^6$ m/s, the calculated n_e value is 10^{13} cm⁻².

References

- [1] R. Wang, J. Xue, K. L. Wang, Z. K. Wang, Y. Luo, D. Fenning, G. Xu, S. Nuryyeva, T. Huang, Y. Zhao, J. L. Yang, J. Zhu, M. Wang, S. Tan, I. Yavuz, K. N. Houk, Y. Yang, Constructive molecular configurations for surface-defect passivation of perovskite photovoltaics, *Science* 366 (2019) 1509.

- [2] J. Siekmann, S. Ravishankar, T. Kirchartz, Apparent defect densities in halide perovskite thin films and single crystals, *ACS Energy Lett.* 6 (2021) 3244.
- [3] J. Wiktor, U. Rothlisberger, A. Pasquarello, Predictive determination of band gaps of inorganic halide perovskites, *J. Phys. Chem. Lett.* 8 (2017) 5507.
- [4] C. A. López, C. Abia, M. C. Alvarez-Galván, B. K. Hong, M. V. Martínez-Huerta, F. Serrano-Sánchez, F. Carrascoso, A. Castellanos-Gómez, M. T. Fernández-Díaz, J. A. Alonso, Crystal structure features of CsPbBr₃ perovskite prepared by mechanochemical synthesis, *ACS Omega* 5 (2020) 5931.
- [5] L. Leppert, T. Rangel, J. B. Neaton, Towards predictive band gaps for halide perovskites: lessons from one-shot and eigenvalue self-consistent GW, *Phys. Rev. Mater.* 3 (2019) 103803.
- [6] W. J. Yin, T. Shi, Y. Yan, Superior photovoltaic properties of lead halide perovskites: insights from first-principles theory, *J. Phys. Chem. C* 119 (2015) 5253.